THE JOURNAL OF PHYSICAL CHEMISTRY C
A JOURNAL OF THE AMERICAN CHEMICAL SOCIETY

pubs.acs.org/JPCC

Article

Ab Initio Molecular Dynamics Simulation Study on Phosphorus/Boron Co-Doped Si Nanocrystals/SiO_2 Core/Shell Structures

Junnan Han, Dongke Li, Jiaming Chen, Teng Sun, Yuhao Wang, Xiaodong Pi, Wei Li, Ling Xu, Jun Xu,* and Kunji Chen

Cite This: *J. Phys. Chem. C* 2023, 127, 17609−17616

Read Online

ACCESS | Metrics & More | Article Recommendations | Supporting Information

ABSTRACT: Co-doping in Si nanocrystals (Si NCs) is an intriguing research topic as the co-doping mechanism at the nanoscale is considerably more complex than the bulk Si. In this study, we utilized ab initio molecular dynamics simulations to investigate the impact of phosphorus (P) and boron (B) co-doping on the properties of Si NCs in the SiO_2 matrix. Our findings demonstrate that P and B impurities exhibit a tendency to aggregate within sub-interfaces and interfacial regions. Furthermore, introducing B impurities during the co-doping process facilitates bonding between P and B near the interface to form P−B pairs. The results of ionic conductivity derived from the diffusion coefficient indicate that with increasing B concentration, the conductance activation energy first decreases before increasing, implying that the introduction of B impurity leads to greater bonding of P impurity to Si or B atoms. Vibrational simulations and bonding configurations on the structure reveal that P−B pair formation weakens the intensity of the vibrational density peak due to the P−B co-doping process, thereby stabilizing the structure.

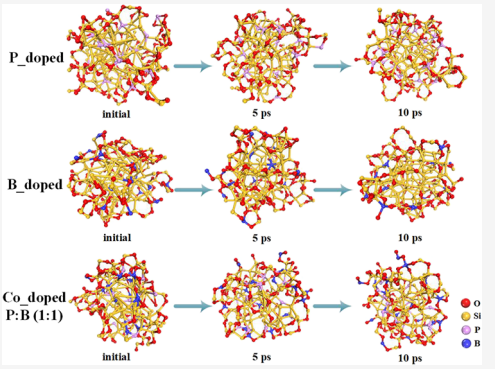

1. INTRODUCTION

Doping in the nanoscale is a critical issue for improving the functionality of Si nanocrystals (Si NCs)-based devices.[1,2] Generally, Si NCs mainly refer to silicon particles with a diameter between 1 and 10 nm and can be formed by a laser or high-temperature annealing process.[3,4] In recent years, the great influence of doping on the performance of Si NCs has attracted extensive attention. Doping offers a promising approach for improving the performance of Si NCs devices, such as enhancing their conductivity,[5] which can be applied to electronic devices. Moreover, doping can also lead to localized surface plasmon resonance in Si NCs,[6,7] which has garnered interest as a potential application in sensing and optoelectronics.[8,9] In our previous study, doping Si NCs with phosphorus (P) or boron (B) can significantly modify their electronic and optical properties. Moreover, we found that the introduction of P impurities can achieve sub-band luminescence and improve the optical properties and can also improve the conductivity by changing the carrier transport behaviors through doping.[10−13] Meanwhile, we also found that P and B co-doping can further improve the sub-band luminescence of Si NCs.[14] To further unravel the underlying doping mechanism governing these phenomena, we leveraged the cutting-edge atom probe tomography technology to conduct meticulous examinations of the positional and distributional aspects of B and P impurities within Si NCs.[15] However, the formation mechanism and distribution of doping impurities and their bonding configuration changes during the annealing process are still unclear.

Ab initio molecular dynamics (AIMD) simulations are a powerful tool that can provide a viable complementary approach to experimental investigations and can effectively surmount the limitations encountered in conventional empirical methods.[16] Several studies have reported on the molecular dynamics of Si NCs, including investigations into freestanding structures outside the encapsulation of hydrogen atoms, as well as models focusing on the encapsulation of N and O within the external environment of Si.[17−20] However, limited research has been conducted on the Si/SiO_2 structure of the core−shell model, which is constructed similarly to our model. Additionally, there has been minimal exploration into the mechanism of co-doping.

In this work, we employ AIMD to investigate the co-doping mechanism of P-doped and P/B co-doped in Si NCs/SiO_2 structures of 2.5 nm. We perform optimization and processing on the structures, followed by doping with varying proportions of P and B. The doped structures undergo amorphization

Received: June 21, 2023
Revised: August 6, 2023
Published: August 23, 2023

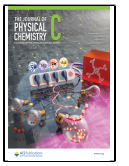

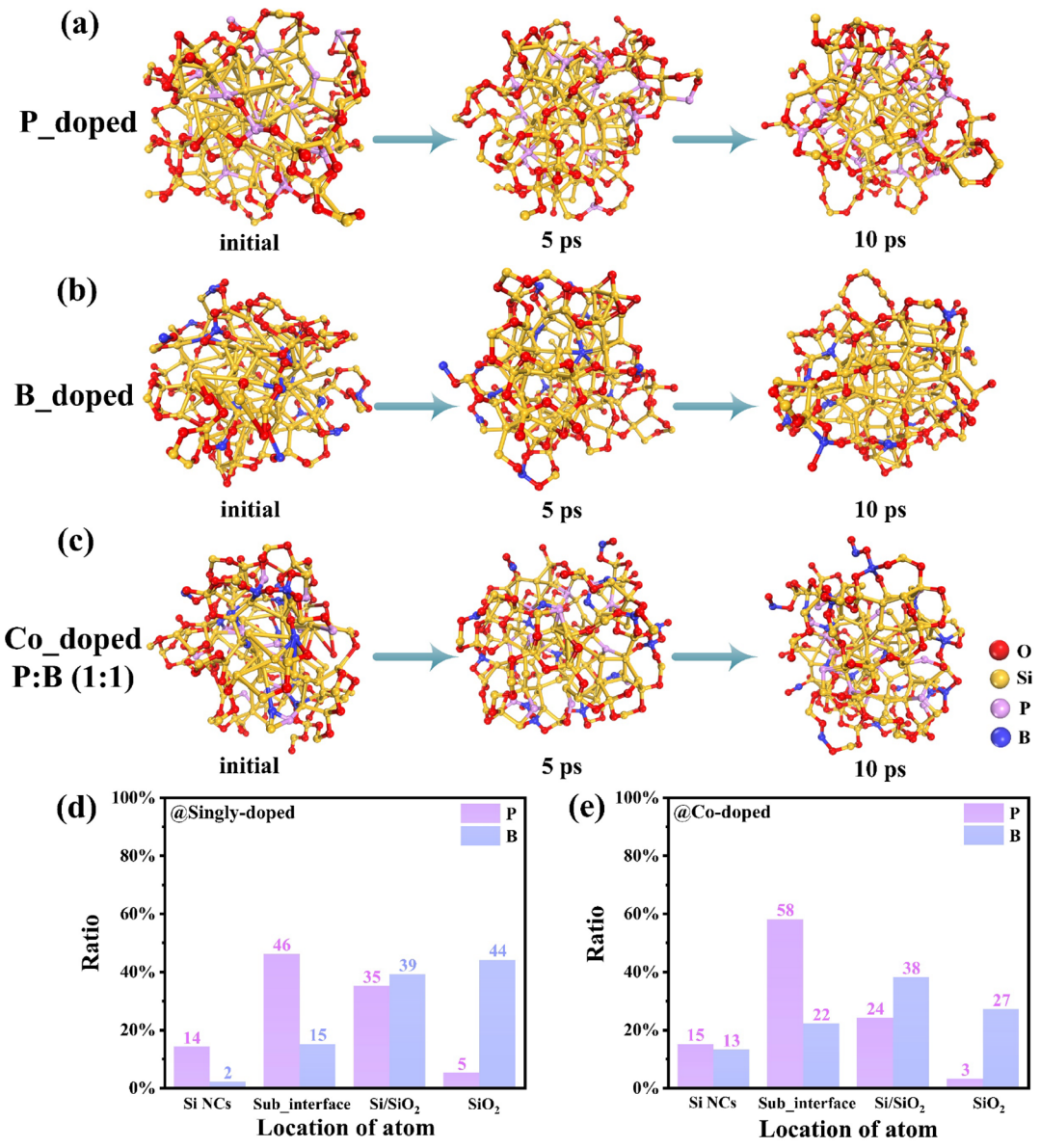

Figure 1. (a–c) Molecular dynamics process of annealing at 1300 K for 10 ps representing for P-doped, B-doped, and co-doped (P:B = 1:1) Si NCs/SiO_2 structures. The red, yellow, purple, and blue balls represent the O atoms, Si atoms, P atoms, and B atoms, respectively. (d, e) Schematic illustration of the atomic position distribution ratio of P/B atoms in singly doped and co-doped Si NCs/SiO_2 structures.

treatment at 3000 K and simulated annealing at 1300 K to show the evolution of the structure and impurity distribution. Our findings reveal that in the co-doped Si NCs/SiO_2 structures, P and B atoms exhibit a strong preference for the sub-interface and interface regions, forming a specific ratio of P/B impurities within the structure. The distribution pattern of P and B atoms is primarily concentrated near the interface, indicating their tendency to form bonds in proximity to the interface. Compared to the singly doped structure, the co-doped structure demonstrates a lower conductance activation energy, while the diffusion coefficient of P atoms gradually increases with temperature, and P/B atoms exhibit varying degrees of diffusion. These results underscore the significance of AIMD simulations in gaining a comprehensive understanding of the microscopic co-doping mechanism of P and B in Si NCs. This study holds promise in advancing the design and development of next-generation nano-electronic devices.

2. COMPUTATIONAL MODELS AND METHODS

In our previous experiments, we successfully fabricated multilayers of doped Si NCs embedded in the SiO_2 matrix, as reported in several scientific publications.[10,21] Notably, the surfaces of Si NCs with varying sizes are enveloped by oxygen, with the outermost layer comprising amorphous SiO_2. Initially, we optimized the structure by hydrogen-bonding capping, followed by dehydrogenation to align with the experimental model. Subsequently, we generated doped models ($Si_{184}O_{110}P_{16}$, $Si_{184}O_{110}B_{16}$, $Si_{168}O_{110}P_{16}B_{16}$, $Si_{176}O_{110}P_{16}B_8$, and $Si_{180}O_{110}P_{16}B_4$) with varying ratios for conducting molecular dynamics simulations. Then, we initiated the amorphization treatment on our 2.5 nm Si NCs/SiO_2 model at a temperature of 3000 K. Subsequently, after the completion of the entire process, we performed an annealing treatment with a temperature gradient. Figure 1a–c shows the kinetic process of our structural model at 1300 K for a duration of 10 ps following amorphization, respectively. Following annealing

https://doi.org/10.1021/acs.jpcc.3c04190
J. Phys. Chem. C 2023, 127, 17609−17616

at 1300 K, the structures exhibited good stability, as evidenced by Figure S1 in the Supporting Information, which provides a comprehensive depiction of the energy and temperature curve variations.

In our work, all AIMD simulations were performed using the density functional theory[22] combined with projector augmented wave potentials,[23] which was performed by the Vienna Ab initio Simulation Package (VASP).[24,25] The electronic wave function was expanded using plane waves, with a cutoff energy of 400 eV. Integrations in the reciprocal space were performed using a Γ-centered grid of k-points, ensuring the smallest spacing between k-points to be 0.5 $Å^{-1}$ within the Brillouin zone corresponding to the primitive cell. To accurately describe electron interactions, the generalized gradient approximation based on the Perdew−Burke−Ernzerhof parametrization was utilized.[26,27] The constant number of atoms, volume, and temperature ensemble was applied with the Nosé−Hoover thermostat.[28,29] The duration of the entire MD process is 10 ps, and the time step is set to 2 fs, and the temperature is set at 300, 500, 800, 1000, and 1300 K. The total energy converged to 10^{-5} eV per cell in each self-consistent loop.

Mean squared displacement (MSD) is a measure of the deviation of the position of a particle with respect to a reference position over time. It can be calculated using the Einstein equation,[30−32] which is expressed as follows:

$$\mathrm{MSD}(r_d) = <\frac{1}{N}\sum_{i=1}^{N} r_d - r_d(t_0)|^2>_{t_0} \quad (1)$$

where N is the number of equivalent particles, r are their coordinates, and d is the desired dimensionality of the MSD.

As in the experiments,[33,34] AIMD simulations can be performed at multiple temperatures to obtain the Arrhenius relation of D as a function of T:

$$D = D_0 \exp\left(-\frac{E_a}{kT}\right) \quad (2)$$

The activation energy E_a can be determined by fitting the data of lg$D$ (logarithm of diffusivity) vs $1/T$ (reciprocal of temperature) to the Arrhenius relationship. This fitting allows for the extrapolation of diffusivity D and conductivity σ to different temperatures. It is important to note that when extrapolating the Arrhenius relationship to other temperatures, it assumes the same diffusion mechanism at those temperatures.

From the diffusivity D, the ionic conductivity σ is calculated by the equation[35]

$$\sigma = \frac{Nq^2}{Vk_BT}D \quad (3)$$

where V is the total volume of the model, q is the charge of the mobile-ion species, T is the temperature, and k_B is the Boltzmann constant.

The radial distribution function (RDF) defines the probability of finding a particle at distance r from another tagged particle. And the $g(r)$ of the RDF can be expressed as follows:

$$g(r) = \frac{L^3}{N^2}\left(\sum_{i=1}^{N}\frac{n(r)}{4\pi^2\Delta r}\right) \quad (4)$$

where L is the length of structures, which have adapted to the change of temperature, N is the total atom number, and $n(r)$ is the number of atoms around one central atom within the distance interval between r and $r + \Delta r$.

The velocity-autocorrelation function (VACF) is a prime example of a time-dependent correlation function and is important because it reveals the underlying nature of the dynamical processes operating in a molecular system. It can be defined as follows:[36]

$$\mathrm{VACF}_M(t) = \frac{1}{N_O N_M}\sum_{j=1}^{N_O}\sum_{i=1}^{N_M} v_i(t_j)\cdot v_i(t_j + t) \quad (5)$$

where v is the velocity vector of atoms and N_O and N_M are the number of time origins spaced by t and number of ions, respectively.

3. RESULTS AND DISCUSSION

As shown in Figure 1, it depicts the AIMD process in both singly doped and co-doped SiO_2/Si NCs structures. The simulation, conducted for a duration of 10 ps, reveals distinct distributions and behaviors of different elements. Specifically, Si exhibits partial crystallization and forms a Si core in the central region. P shows a more dispersed distribution in the sublayer and at the Si/SiO_2 interface. On the other hand, B is mainly concentrated at the interface and forms bonds with oxygen atoms in SiO_2. Furthermore, Figure 1 illustrates the formation of P−B pairs near the Si/SiO_2 interface. This is consistent with some previous experimental results.[15,37,38] To further analyze the distribution of dopant atoms in Si, we conducted a thorough investigation of the distribution ratio of impurity atoms. In Figure 1d, the results illustrate that following the AIMD process, 46% of the P atoms are distributed at the sub-interface in the singly doped SiO_2/Si NCs structures, while 35% are found at the Si/SiO_2 interface. Meanwhile, only 14% of the P atoms are distributed within the Si NCs, and a mere 5% within the SiO_2 layer. These findings clearly indicate the preference of P atoms to reside in sublayers and interfaces, with only a small fraction being successfully doped into the center of Si NCs to form bonds with Si. It is worth noting that it is difficult for P atoms to enter the SiO_2 layer. Unlike P atoms, 44 and 39% of B atoms are distributed near the SiO_2 and Si/SiO_2 interfaces and only 2% are distributed in Si NCs. This also shows that B impurities are more difficult to dope into Si NCs but tend to exist at the interfacial regions and SiO_2.

As for the co-doped case, Figure 1e depicts the distribution proportions of P and B atoms that differ across various positions within the co-doped SiO_2/Si NCs structures. At the sub-interface position, P atoms constitute 58% of the distribution, while B atoms account for 22%. Moving to the Si/SiO_2 interface, the distribution ratios shift to 24% for P atoms and 38% for B atoms. Within the Si NCs, the proportions of P and B atoms are comparatively lower at 15 and 13%, respectively. However, in the SiO_2 layer, the distribution ratio of B atoms is 27%, while P atoms only comprise 3%.

These results suggest that in the case of co-doping, P and B atoms still tend to be distributed in sub-interfaces and interfacial regions. Additionally, compared with P, a part of B atoms is still in SiO_2, which is also consistent with the phenomenon found in the experiment that B atoms gather in SiO_2 to form a shell. Overall, the distribution pattern of P and

https://doi.org/10.1021/acs.jpcc.3c04190
J. Phys. Chem. C 2023, 127, 17609−17616

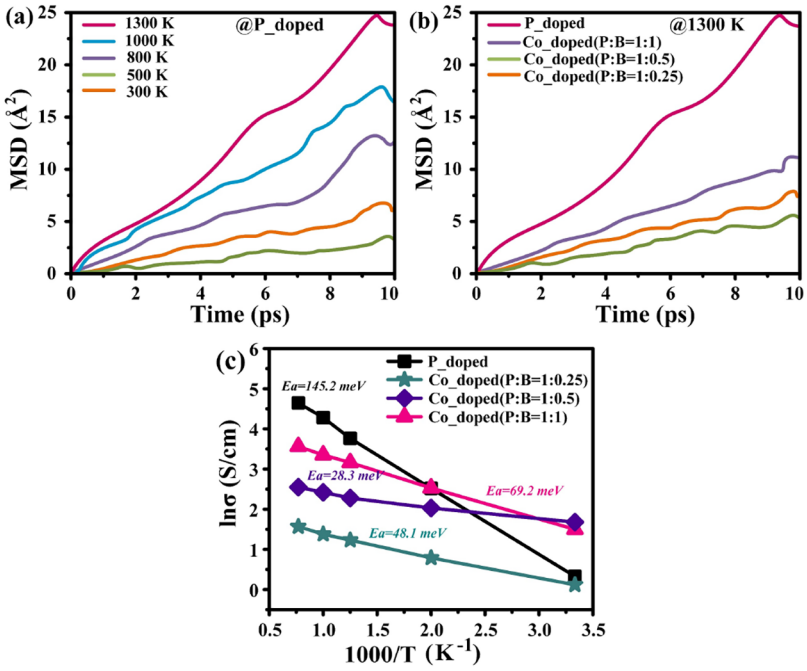

Figure 2. (a) MSD of P atoms as a function of time increment for different thermodynamic temperatures. (b) MSD of P/B atoms as a function of time increment for P-doped and co-doped Si NCs/SiO_2 structures. (c) Temperature-dependent lnσ plot for P-doped and co-doped Si NCs/SiO_2 structures.

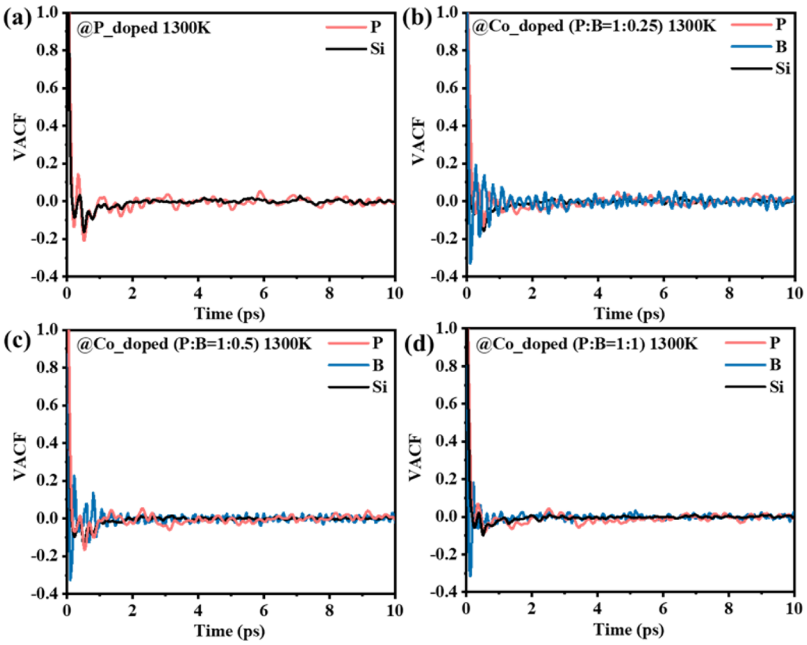

Figure 3. (a–d) VACF of Si, P/B atoms in singly doped and co-doped Si NCs/SiO_2 structures. The simulations have been performed in the thermodynamic at a temperature of T = 1300 K.

B atoms in the co-doped SiO_2/Si NCs structures concentrates near the interface. This observation aligns with the notion that P and B atoms tend to form bonds in close proximity to the interface, particularly the formation of the P−B pair. Additionally, the distribution of P atoms near the interface region contributes to an enhanced proportion of impurity atoms doped into the interior of Si NCs.

To investigate the dynamical properties of SiO_2/Si NCs structures, we computed the MSD of P atoms at different temperatures for singly doped and compared the MSD of P/B atoms under co-doped SiO_2/Si NCs structures with different ratios. Figure 2a suggests that the MSD curve of the P atom exhibits a linear increase over time, implying continuous diffusion of P atoms within the structures and an escalation in diffusion intensity as the temperature increases. This is because impurity atoms tend to find more stable positions to bond with surrounding atoms, and the diffusion coefficient of atomic motion changes with temperature. Figure 2b shows that P atoms with singly doped exhibit a greater diffusion coefficient at a fixed temperature of 1300 K with the passage of time.

https://doi.org/10.1021/acs.jpcc.3c04190
J. Phys. Chem. C 2023, 127, 17609−17616

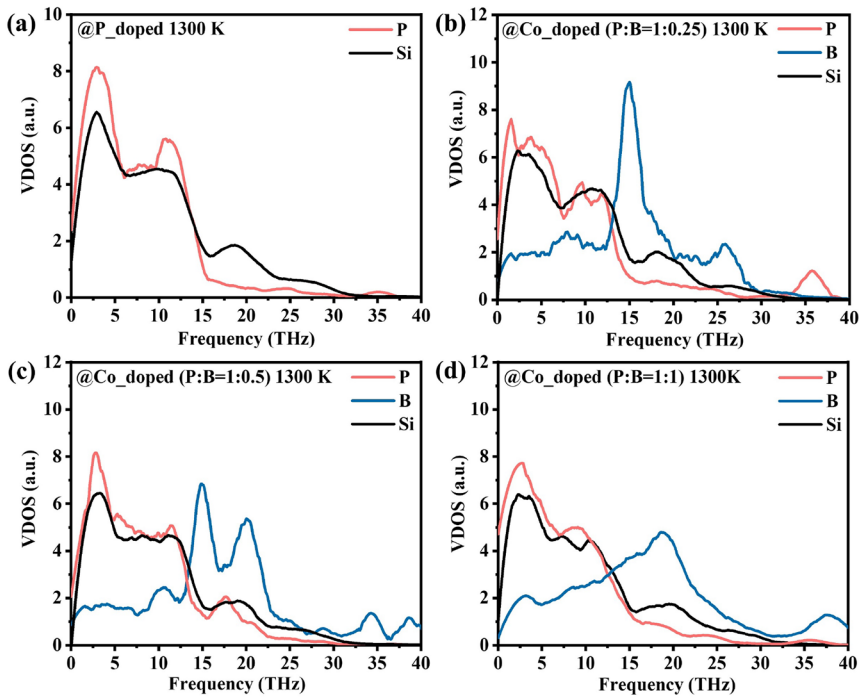

Figure 4. (a–d) Vibrational density of states (VDOS) of Si, P/B atoms in singly doped and co-doped Si NCs/SiO_2 structures. The simulations have been performed in the thermodynamic at a temperature of T = 1300 K.

Moreover, the diffusion degree is higher for co-doped P and B in a 1:1 proportion as compared with those in ratios of 1:0.5 and 1:0.25. It is worth noting that the slope of the MSD of impurity atoms is found to be smaller at the P–B co-doped ratio of 1:0.5 compared to the P–B co-doped ratio of 1:0.25. Therefore, we speculate that the gradual bonding of P and B atoms at a certain doping ratio leads to a decrease in MSD, while an increase in the number of atoms at higher doping ratios causes a further increase in MSD.

To further understand the changes of ionic conductivity σ of singly doped and co-doped Si NCs/SiO_2 structures, we performed the process of AIMD in the temperature range of 300–1300 K and analyzed the results. The lnσ curves of the diffusion coefficient versus temperature are shown in Figure 2c. The linear relationship between the conductivity and the reciprocal of the temperature can be observed, which is described as with the Arrhenius relationship, which is also consistent with the carrier transport mechanism of Si NCs in the experiment.[10,13] Figure 2c reveals that the singly doped structures have a higher conductivity activation energy (E_a) than the co-doped structures. This indicates that the diffusion of dopant atoms in the co-doped structures leads to the existence of more carriers. Thus, as more donors or acceptors are introduced into Si NCs, the Fermi level shifts. In particular, when the ratio of P to B is 1:0.5, the value of E_a is as low as 28.3 meV. It is speculated that this may be due to the reduction of carriers caused by P–B bonding at high-concentration co-doping at this time. Compared with a P:B ratio of 1:0.25, the lower concentration of B doping results in insufficient carrier concentration. The overall E_a value of 28.3–145.2 meV is due to the smaller Si NCs structure, which makes it more difficult to dope impurity atoms, resulting in a larger E_a value. This is also consistent with the results observed in the experiment.[39,40]

To better study the origin of interactions between impurity atoms and Si atoms, we plot the VACF for the Si, P/B atoms in singly doped and co-doped Si NCs/SiO_2 structures. The VACF analysis of the AIMD process is used to study the change in the interaction strength between the dopant atom and the surrounding bonded atomic grid, where the negative value of the VACF curve indicates that the dopant atom is bonded to the surrounding atoms. In Figure 3a, at the initial position of the time-dependent function, the VACF of P atoms has a larger amplitude vibration than Si, and the vibration decays to zero slower.[41] Figure 3b–d demonstrates that in the co-doped structures, when the doping ratio of P atoms is fixed, as the B doping concentration increases, the VACF amplitudes of both B and P atoms decrease, which also proves that the P atom is the reason for forming a bond with the B atom to form P–B pairs. Overall, the gradual weakening of the oscillation frequency of the VACF curve indicates the stability of the structure and the relative stability of the atomic position.

The VDOS was calculated as Fourier transform of the VACF, as shown in Figure 4a–d. The VDOS curve of Si atoms in the terahertz range of 0–15 THz shows stable peak positions and intensities for both transverse acoustic mode and longitudinal acoustic mode.[41–43] However, the position of the longitudinal optical mode peak at 19 THz is slightly increased, while the higher-frequency transverse optical mode peak is small due to the small size of Si NCs/SiO_2 structures (approximately 2.5 nm). The VDOS curve of P impurities is similar to that of Si, indicating stability in both singly doped and co-doped structures. On the other hand, the VDOS curve of B impurities exhibits an increase in peak intensity at the position of 15 THz when doped at a low concentration. Figure 4b–d reveals that with the increase of B concentration, the intensity of the VDOS peak of B at 25 THz decreases, and the range of the peak also broadens between 15 and 20 THz. These results indicate that B atoms vibrate more vigorously at

https://doi.org/10.1021/acs.jpcc.3c04190
J. Phys. Chem. C 2023, 127, 17609–17616

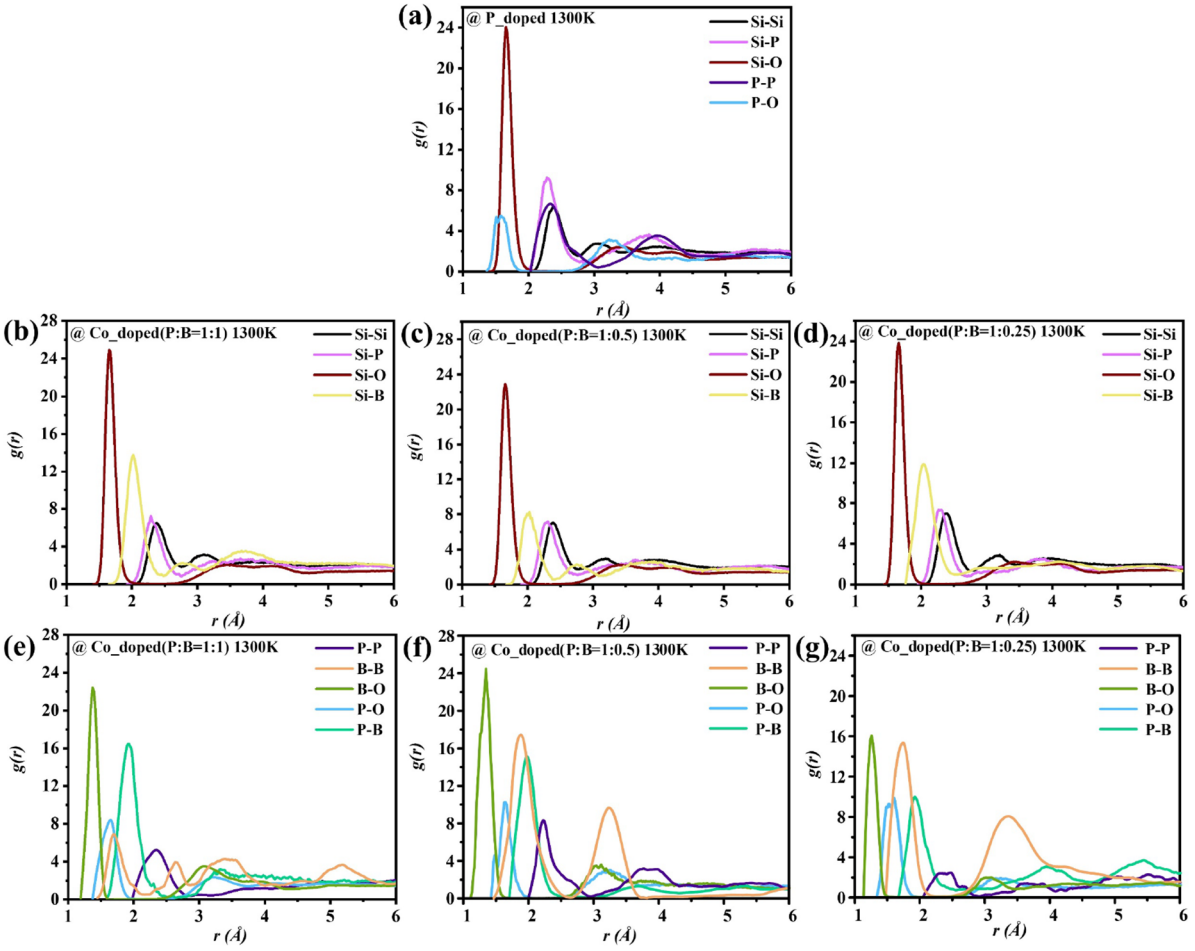

Figure 5. (a–g) RDF of Si-X (X = Si, P, B, and O), P-X (X = P and O), and B-X (X = B and O) in singly doped and co-doped Si NCs/SiO_2 structures at T = 1300 K.

low doping concentrations, and the degree of bonding with P atoms and Si atoms increases with increasing doping concentrations. Furthermore, P–B pairs are more likely to exist when the concentrations of P and B are consistent, which reduces the intensity of the VDOS.

To better understand the bonding configuration of the Si NCs/SiO_2 structures, we further calculated the RDF between atoms. Figure 5a–d shows that the first peak position of the Si–Si RDF is around 2.3–2.5 Å, indicating the formation of Si–Si bonds through Si crystallization. The second peak position is around 3–4.3 Å. This distribution corresponds to the Si–Si bond distribution in amorphous silicon and the Si–Si bond distribution in the amorphous SiO_2 matrix, which is consistent with results reported in the literature.[44,45] The first peak position of the Si–O RDF is around 1.6–1.7 Å, which is consistent with the bond length of the Si–O bond at around 1.6 Å. Overall, the minimal change at a temperature of 1300 K demonstrates the stability of the SiO_2 matrix. With the doping of P impurity atoms, the RDF of Si–P is observed to be between 2.2 and 2.3 Å, indicating the formation of Si–P bonds. Additionally, the RDF of P–P is also observed in the singly doped structures, which is also in good agreement with the P–P bond lengths (2.2–2.25 Å).[46] On the other hand, for the Si–B RDF, the peak position around 2 Å indicates the formation of Si–B bonds (1.8–2 Å). The formation of Si–B bonds also corresponds to the change trend of the Si–B–Si bond angle, as shown in Figure S2. The Si–B RDF peak tends to decrease first and then increase with increasing doping concentration. This also confirms the previous analysis of P–B pair formation. In the co-doped structures, the B–B RDF peak is observed to be around 1.6–1.8 Å, corresponding to the formation of B–B bonds. This can also explain the aggregation of B atoms observed in the experiment into a shell.[15,37] At the same time, the RDF peak of B–O around 1.3 Å corresponds to the formation of B–O bonds, with the larger peak indicating that B is more likely to exist at the Si/SiO_2 interface and SiO_2 matrix and form bonds with O atoms. As the B doping concentration increases, the RDF intensity of B–B decreases while that of P–B increases, indicating the formation of P–B bonds. Additionally, the peak positions and intensities of the RDF of P–O and B–O remain relatively stable, suggesting that impurities bonded to O atoms near the interface are stable. These results are consistent with experimental observations and provide a theoretical explanation for the doping mechanism.[15,37]

4. CONCLUSIONS

In summary, we investigated the effect of temperature-dependent P/B co-doping on Si NCs using the AIMD simulation method. Our study shows that both P and B atoms tend to aggregate at sub-interfaces and interfacial regions in general. Moreover, P atoms are more tightly distributed near the sub-interface, while B atoms are more widely distributed at the Si/SiO_2 interface and in SiO_2,

https://doi.org/10.1021/acs.jpcc.3c04190
J. Phys. Chem. C 2023, 127, 17609–17616

consistent with the experimental observations. The introduction of B impurities facilitates bonding between P and B near the interface to form a P−B pair. Furthermore, we found that P-doped and P/B co-doped significantly affect the ionic conductivity of Si NCs differently. The results reveal that the co-doped structure exhibits a lower conductivity activation energy than the P-doped structure. Interestingly, with increasing B concentration, the conductivity activation energy initially decreases before increasing, indicating that the introduction of B impurities leads to more bonding of P impurities with Si or B atoms. Moreover, the results of the vibration simulation show that the presence of P−B pairs weakens the intensity of the vibration density peak, thereby stabilizing the structure. Finally, our study of bonding configurations indicates that the P/B co-doped structure tends to form P−B bonds near the interface region more likely than the P-doped structure.

■ ASSOCIATED CONTENT

Supporting Information

The Supporting Information is available free of charge at https://pubs.acs.org/doi/10.1021/acs.jpcc.3c04190.

(Figure S1) Total energy and temperature; (Figure S2) distribution of bond angles (PDF)

■ AUTHOR INFORMATION

Corresponding Author

Jun Xu − *National Laboratory of Solid State Microstructures, School of Electronic Science and Engineering, Collaborative Innovation Center of Advanced Microstructures, Jiangsu Provincial Key Laboratory of Advanced Photonic and Electronic Materials, Nanjing University, Nanjing 210093, China;* orcid.org/0000-0002-0469-9766; Email: junxu@nju.edu.cn

Authors

Junnan Han − *National Laboratory of Solid State Microstructures, School of Electronic Science and Engineering, Collaborative Innovation Center of Advanced Microstructures, Jiangsu Provincial Key Laboratory of Advanced Photonic and Electronic Materials, Nanjing University, Nanjing 210093, China;* orcid.org/0000-0003-4476-040X

Dongke Li − *National Laboratory of Solid State Microstructures, School of Electronic Science and Engineering, Collaborative Innovation Center of Advanced Microstructures, Jiangsu Provincial Key Laboratory of Advanced Photonic and Electronic Materials, Nanjing University, Nanjing 210093, China; Zhejiang Provincial Key Laboratory of Power Semiconductor Materials and Devices, ZJU-Hangzhou Global Scientific and Technological Innovation Center, School of Materials Science and Engineering, Zhejiang University, Hangzhou 311200, China*

Jiaming Chen − *National Laboratory of Solid State Microstructures, School of Electronic Science and Engineering, Collaborative Innovation Center of Advanced Microstructures, Jiangsu Provincial Key Laboratory of Advanced Photonic and Electronic Materials, Nanjing University, Nanjing 210093, China*

Teng Sun − *National Laboratory of Solid State Microstructures, School of Electronic Science and Engineering, Collaborative Innovation Center of Advanced Microstructures, Jiangsu Provincial Key Laboratory of Advanced Photonic and Electronic Materials, Nanjing University, Nanjing 210093, China*

Yuhao Wang − *National Laboratory of Solid State Microstructures, School of Electronic Science and Engineering, Collaborative Innovation Center of Advanced Microstructures, Jiangsu Provincial Key Laboratory of Advanced Photonic and Electronic Materials, Nanjing University, Nanjing 210093, China*

Xiaodong Pi − *State Key Laboratory of Silicon Materials & School of Materials Science and Engineering and Institute of Advanced Semiconductors, Hangzhou Innovation Center, Zhejiang University, Hangzhou 310027, China;* orcid.org/0000-0002-4233-6181

Wei Li − *National Laboratory of Solid State Microstructures, School of Electronic Science and Engineering, Collaborative Innovation Center of Advanced Microstructures, Jiangsu Provincial Key Laboratory of Advanced Photonic and Electronic Materials, Nanjing University, Nanjing 210093, China*

Ling Xu − *National Laboratory of Solid State Microstructures, School of Electronic Science and Engineering, Collaborative Innovation Center of Advanced Microstructures, Jiangsu Provincial Key Laboratory of Advanced Photonic and Electronic Materials, Nanjing University, Nanjing 210093, China*

Kunji Chen − *National Laboratory of Solid State Microstructures, School of Electronic Science and Engineering, Collaborative Innovation Center of Advanced Microstructures, Jiangsu Provincial Key Laboratory of Advanced Photonic and Electronic Materials, Nanjing University, Nanjing 210093, China*

Complete contact information is available at: https://pubs.acs.org/10.1021/acs.jpcc.3c04190

Notes

The authors declare no competing financial interest.

■ ACKNOWLEDGMENTS

This work is supported by the National Key R&D Program of China (2018YFB2200101), NSFC (62004078 and 61921005), and NSF of Jiangsu Province (BK20201073).

■ REFERENCES

(1) Norris, D. J.; Efros, A. L.; Erwin, S. C. Doped Nanocrystals. *Science* **2008**, *319*, 1776−1779.

(2) Arduca, E.; Perego, M. Doping of Silicon Nanocrystals. *Mater. Sci. Semicond. Process.* **2017**, *62*, 156−170.

(3) Švrček, V.; Sasaki, T.; Shimizu, Y.; Koshizaki, N. Blue Luminescent Silicon Nanocrystals Prepared by Ns Pulsed Laser Ablation in Water. *Appl. Phys. Lett.* **2006**, *89*, No. 213113.

(4) Jambois, O.; Rinnert, H.; Devaux, X.; Vergnat, M. Influence of the Annealing Treatments on the Luminescence Properties of SiO/SiO_2 Multilayers. *J. Appl. Phys.* **2006**, *100*, No. 123504.

(5) Stegner, A. R.; Pereira, R. N.; Klein, K.; Lechner, R.; Dietmueller, R.; Brandt, M. S.; Stutzmann, M.; Wiggers, H. Electronic Transport in Phosphorus-Doped Silicon Nanocrystal Networks. *Phys. Rev. Lett.* **2008**, *100*, No. 026803.

(6) Agrawal, A.; Cho, S. H.; Zandi, O.; Ghosh, S.; Johns, R. W.; Milliron, D. J. Localized Surface Plasmon Resonance in Semiconductor Nanocrystals. *Chem. Rev.* **2018**, *118*, 3121−3207.

(7) Liu, X.; Swihart, M. T. Heavily-Doped Colloidal Semiconductor and Metal Oxide Nanocrystals: An Emerging New Class of Plasmonic Nanomaterials. *Chem. Soc. Rev.* **2014**, *43*, 3908−3920.

(8) Cosentino, S.; Mirabella, S.; Liu, P.; Le, S. T.; Miritello, M.; Lee, S.; Crupi, I.; Nicotra, G.; Spinella, C.; Paine, D.; Terrasi, A.; Zaslavsky, A.; Pacifici, D. Role of Ge Nanoclusters in the Performance of Photodetectors Compatible with Si Technology. *Thin Solid Films* **2013**, *548*, 551−555.
(9) Yu, Z.; Aceves-Mijares, M. A Ultraviolet-Visible-near Infrared Photodetector Using Nanocrystalline Si Superlattice. *Appl. Phys. Lett.* **2009**, *95*, No. 081101.
(10) Chen, J.; Li, D.; Zhang, Y.; Jiang, Y.; Xu, J.; Chen, K. Comparative Study on P and B Doped Nano-Crystalline Si Multilayers. *Appl. Surf. Sci.* **2020**, *529*, No. 146971.
(11) Shan, D.; Ji, Y.; Li, D.; Xu, J.; Qian, M.; Xu, L.; Chen, K. Enhanced Carrier Mobility in Si Nano-Crystals via Nanoscale Phosphorus Doping. *Appl. Surf. Sci.* **2017**, *425*, 492−496.
(12) Li, D.; Jiang, Y.; Liu, J.; Zhang, P.; Xu, J.; Li, W.; Chen, K. Modulation of Surface States by Phosphorus to Improve the Optical Properties of Ultra-Small Si Nanocrystals. *Nanotechnology* **2017**, *28*, No. 475704.
(13) Qian, M.; Shan, D.; Ji, Y.; Li, D.; Xu, J.; Li, W.; Chen, K. Transition of Carrier Transport Behaviors with Temperature in Phosphorus-Doped Si Nanocrystals/SiO_2 Multilayers. *Nanoscale Res. Lett.* **2016**, *11*, 346.
(14) Li, D.; Chen, J.; Sun, T.; Zhang, Y.; Xu, J.; Li, W.; Chen, K. Enhanced Subband Light Emission from Si Quantum Dots/SiO_2 Multilayers via Phosphorus and Boron Co-Doping. *Opt. Express* **2022**, *30*, 12308.
(15) Li, D.; Chen, J.; Xue, Z.; Sun, T.; Han, J.; Chen, W.; Talbot, E.; Demoulin, R.; Li, W.; Xu, J.; Chen, K. Atomic-Scale Study on the Dopant Distribution in Phosphorus and Boron-Doped Si Nanocrystals/SiO_2 Multilayers. *Appl. Surf. Sci.* **2023**, *609*, No. 155260.
(16) Hehre, W. J. Ab Initio Molecular Orbital Theory. *Acc. Chem. Res.* **1976**, *9*, 399−406.
(17) Peng, W.-T.; Fales, B. S.; Shu, Y.; Levine, B. G. Dynamics of Recombination via Conical Intersection in a Semiconductor Nanocrystal. *Chem. Sci.* **2018**, *9*, 681−687.
(18) Turanský, R.; Brndiar, J.; Pershin, A.; Gali, Á.; Sugimoto, H.; Fujii, M.; Štich, I. Structure and Properties of Heavily B and P Codoped Amorphous Silicon Quantum Dots. *J. Phys. Chem. C* **2021**, *125*, 23267−23274.
(19) Qian, Y.; Du, Z.; Zhu, R.; Wu, H.; Kan, E.; Deng, K. Atomically Thin Mononitrides SiN and GeN: New Two-Dimensional Wide Band Gap Semiconductors. *EPL Europhys. Lett.* **2018**, *122*, 47002.
(20) Khalilov, U.; Pourtois, G.; Bogaerts, A.; Duin, A. C. T.; Neyts, E. C. Reactive Molecular Dynamics Simulations on SiO_2 -Coated Ultra-Small Si-Nanowires. *Nanoscale* **2013**, *5*, 719−725.
(21) Li, D.; Jiang, Y.; Zhang, P.; Shan, D.; Xu, J.; Li, W.; Chen, K. The Phosphorus and Boron Co-Doping Behaviors at Nanoscale in Si Nanocrystals/SiO $_2$ Multilayers. *Appl. Phys. Lett.* **2017**, *110*, No. 233105.
(22) Parr, R. G. Density Functional Theory. *Annu. Rev. Phys. Chem.* **1983**, *34*, 631−656.
(23) Kresse, G.; Joubert, D. From Ultrasoft Pseudopotentials to the Projector Augmented-Wave Method. *Phys. Rev. B* **1999**, *59*, 1758−1775.
(24) Kresse, G.; Furthmüller, J. Efficient Iterative Schemes for Ab Initio Total-Energy Calculations Using a Plane-Wave Basis Set. *Phys. Rev. B* **1996**, *54*, 11169−11186.
(25) Wang, V.; Xu, N.; Liu, J.-C.; Tang, G.; Geng, W.-T. VASPKIT: A User-Friendly Interface Facilitating High-Throughput Computing and Analysis Using VASP Code. *Comput. Phys. Commun.* **2021**, *267*, No. 108033.
(26) Perdew, J. P.; Burke, K.; Ernzerhof, M. Generalized Gradient Approximation Made Simple. *Phys. Rev. Lett.* **1996**, *77*, 3865−3868.
(27) Hammer, B.; Hansen, L. B.; Nørskov, J. K. Improved Adsorption Energetics within Density-Functional Theory Using Revised Perdew-Burke-Ernzerhof Functionals. *Phys. Rev. B* **1999**, *59*, 7413−7421.
(28) Andersen, H. C. Molecular Dynamics Simulations at Constant Pressure and/or Temperature. *J. Chem. Phys.* **1980**, *72*, 2384−2393.
(29) Evans, D. J.; Holian, B. L. The Nose−Hoover Thermostat. *J. Chem. Phys.* **1985**, *83*, 4069−4074.
(30) He, X.; Zhu, Y.; Epstein, A.; Mo, Y. Statistical Variances of Diffusional Properties from Ab Initio Molecular Dynamics Simulations. *npj Comput. Mater.* **2018**, *4*, 18.
(31) Iftimie, R.; Minary, P.; Tuckerman, M. E. Ab Initio Molecular Dynamics: Concepts, Recent Developments, and Future Trends. *Proc. Natl. Acad. Sci.* **2005**, *102*, 6654−6659.
(32) Dunderdale, G.; Ebbens, S.; Fairclough, P.; Howse, J. Importance of Particle Tracking and Calculating the Mean-Squared Displacement in Distinguishing Nanopropulsion from Other Processes. *Langmuir* **2012**, *28*, 10997−11006.
(33) Kamaya, N.; Homma, K.; Yamakawa, Y.; Hirayama, M.; Kanno, R.; Yonemura, M.; Kamiyama, T.; Kato, Y.; Hama, S.; Kawamoto, K.; Mitsui, A. A Lithium Superionic Conductor. *Nat. Mater.* **2011**, *10*, 682−686.
(34) Kosova, N. V.; Devyatkina, E. T.; Stepanov, A. P.; Buzlukov, A. L. Lithium Conductivity and Lithium Diffusion in NASICON-Type $Li_{1+x}Ti_{2-x}Al_x(PO_4)_3$ (X= 0; 0.3) Prepared by Mechanical Activation. *Ionics* **2008**, *14*, 303−311.
(35) Marcolongo, A.; Marzari, N. Ionic Correlations and Failure of Nernst-Einstein Relation in Solid-State Electrolytes. *Phys. Rev. Mater.* **2017**, *1*, No. 025402.
(36) Alder, B. J.; Wainwright, T. E. Decay of the Velocity Autocorrelation Function. *Phys. Rev. A* **1970**, *1*, 18−21.
(37) Nomoto, K.; Sugimoto, H.; Breen, A.; Ceguerra, A. V.; Kanno, T.; Ringer, S. P.; Wurfl, I. P.; Conibeer, G.; Fujii, M. Atom Probe Tomography Analysis of Boron and/or Phosphorus Distribution in Doped Silicon Nanocrystals. *J. Phys. Chem. C* **2016**, *120*, 17845−17852.
(38) Nomoto, K.; Sugimoto, H.; Cui, X.-Y.; Ceguerra, A. V.; Fujii, M.; Ringer, S. P. Distribution of Boron and Phosphorus and Roles of Co-Doping in Colloidal Silicon Nanocrystals. *Acta Mater.* **2019**, *178*, 186−193.
(39) Jiang, Y.; Li, D.; Xu, J.; Li, W.; Chen, K. Size-Dependent Phosphorus Doping Effect in Nanocrystalline-Si-Based Multilayers. *Appl. Surf. Sci.* **2018**, *461*, 66−71.
(40) Rui, Y.; Li, S.; Xu, J.; Song, C.; Jiang, X.; Li, W.; Chen, K.; Wang, Q.; Zuo, Y. Size-Dependent Electroluminescence from Si Quantum Dots Embedded in Amorphous SiC Matrix. *J. Appl. Phys.* **2011**, *110*, No. 064322.
(41) Tilocca, A. Structure and Dynamics of Bioactive Phosphosilicate Glasses and Melts from Ab Initio Molecular Dynamics Simulations. *Phys. Rev. B* **2007**, *76*, No. 224202.
(42) Hu, M.; Zhang, X.; Giapis, K. P.; Poulikakos, D. Atomistic Mechanisms of Enhancing Energy Conversion Efficiency of Nanostructured Thermoelectrics. In *Volume 4: Energy Systems Analysis, Thermodynamics and Sustainability; Combustion Science and Engineering; Nanoengineering for Energy, Parts A and B*; American Society of Mechanical Engineers Digital Collection, 2011; *pp.* 1695−1702.
(43) Meyer, R.; Comtesse, D. Vibrational Density of States of Silicon Nanoparticles. *Phys. Rev. B* **2011**, *83*, No. 014301.
(44) Kim, S.; Park, J.-S.; Chang, K. J. Stability and Segregation of B and P Dopants in Si/SiO_2 Core−Shell Nanowires. *Nano Lett.* **2012**, *12*, 5068−5073.
(45) Lee, S.-E.; Lim, H.-K.; Lee, S. Ab Initio-Based Structural and Thermodynamic Aspects of the Electrochemical Lithiation of Silicon Nanoparticles. *Catalysts* **2020**, *10*, 8.
(46) Protasiewicz, J. D.; Washington, M. P.; Gudimetla, V. B.; Payton, J. L.; Cather Simpson, M. A Closer Look at the Phosphorus−Phosphorus Double Bond Lengths in Meta-Terphenyl Substituted Diphosphenes. *Inorg. Chim. Acta* **2010**, *364*, 39−45.

https://doi.org/10.1021/acs.jpcc.3c04190
J. Phys. Chem. C 2023, 127, 17609−17616